

THE WEIGHT OF EMPTINESS: THE GRAVITATIONAL LENSING SIGNAL OF STACKED VOIDS

ELISABETH KRAUSE^{1,2}, TZU-CHING CHANG³, OLIVIER DORÉ^{4,1}, AND KEIICHI UMETSU³

(Dated: November 7, 2012)
Draft version November 7, 2012

ABSTRACT

The upcoming new generation of spectroscopic galaxy redshift surveys will provide large samples of cosmic voids, the distinct, large underdense structures in the universe. Combining these with future galaxy imaging surveys, we study the prospects of probing the underlying matter distribution in and around cosmic voids via the weak gravitational lensing effects of stacked voids, utilizing both shear and magnification information. The statistical precision is greatly improved by stacking together a large number of voids along different lines of sight, even when taking into account the impact of inherent miscentering and projection effects. We show that Dark Energy Task Force (DETF) Stage IV surveys, such as the Euclid satellite and the Large Synoptic Survey Telescope (LSST), should be able to detect the void lensing signal with sufficient precision from stacking abundant medium-sized voids, thus providing direct constraints on the matter density profile of voids independent of assumptions on galaxy bias.

Subject headings: cosmology – large scale structure – dark matter – gravitational lensing: weak

1. INTRODUCTION

As revealed by galaxy redshift surveys, the large-scale structure of the universe hierarchically grows into a complex network of filaments and galaxy clusters, separated by large, nearly empty voids in between. While the bound structures contain most of the mass in the Universe, most of the cosmic volume is filled with voids. These voids originate from local minima of the primordial density field and expand faster than the average density of the Universe, clearing out their central regions and building up filaments at their boundaries.

Just as the more studied galaxy clusters, the formation and evolution of voids probe the extreme tails of the cosmic density distribution, and provide insights into initial conditions and the expansion history of the Universe. For example, the abundance of massive clusters and large voids increases in $f(R)$ gravity models (Li et al. 2012), and non-Gaussian initial conditions change the void and cluster abundance in opposite directions (Kamionkowski et al. 2009).

Besides, as the dynamics of underdense regions is dominated by dark energy at earlier times than the rest of the universe, the potential of voids to probe the nature of dark energy has been noted recently. Lavaux & Wandelt (2011) proposed an Alcock-Paczynski test on the average shape of stacked voids and found that it may outperform the Baryonic Acoustic Oscillation effect as a cosmological probe for a Euclid-like survey. In addition, the distribution of void ellipticities has been demonstrated to be a powerful probe of the equation of state of dark energy (Park & Lee 2007; Lavaux & Wandelt 2010; Bos et al. 2012). Similarly, the emptiness of voids and its evolution over cosmic time can probe the expansion history of the universe and modified gravity (e.g., Farrar & Peebles 2004; Nusser et al. 2005; Peebles & Nusser 2010).

Observationally, voids are identified in the distribution of

galaxies (e.g., Sutter et al. 2012, and references therein), and the matter density profile of voids is inferred from the galaxy distribution in and around voids. The latter requires assumptions on galaxy biasing, which is not precisely known and subject to uncertainties in the efficiency of galaxy formation and evolution in underdense environments.

In this *letter* we demonstrate that the matter density profile of voids can instead be constrained directly from the average lensing signal of stacked voids. While weak lensing by voids was previously discussed by Amendola et al. (1999), these authors focused on the tangential shear signals by individual voids and concluded that void radii larger than $\sim 100 \text{ Mpc } h^{-1}$ were required to detect the effect. Compared to their analysis, stacking allows us to achieve much higher significance in measuring the weak lensing signals induced by more abundant, smaller voids. Large number of voids will be available from future spectroscopic galaxy redshift surveys, such as the proposed Prime Focus Spectrograph (PFS; Ellis et al. 2012) instrument on the Subaru telescope and the Euclid satellite; while several future imaging surveys, e.g., the on-going Subaru Hyper Suprime Cam (HSC), Euclid, and the LSST projects, will allow us to measure the stacked weak lensing signals by voids. Such direct measurements of void density profiles enable cosmological constraints without the uncertainties from galaxy biasing models, and may additionally help in studying the environment dependence of galaxy evolution.

2. METHODS AND MODELS

We now forecast the sensitivity of stacked weak lensing of voids and its ability to measure the average density profile of voids. We consider voids in the redshift range of $0.4 < z_1 < 0.6$, assuming the void catalog is available in a survey area of $A = 5000$ square degrees. We also assume a DETF Stage IV deep imaging survey (Albrecht et al. 2006) of the same area for the lensing analysis; the mean background density of galaxies is assumed to be $n_{\text{gal}} = 12 \text{ arcmin}^{-2}$, with a mean redshift of $z_s \sim 1$. Additionally, we consider two specific upcoming surveys: the combination of HSC and PFS, known

¹ Caltech, Department of Astrophysics, MC 249-17, Pasadena, CA 91125, USA

² University of Pennsylvania, Department of Physics and Astronomy, Philadelphia, PA 19104, USA

³ IAA, Academia Sinica, P.O. Box 23-141, Taipei 10617, Taiwan

⁴ NASA Jet Propulsion Laboratory, California Institute of Technology, 4800 Oak Grove Drive, Pasadena, California, USA

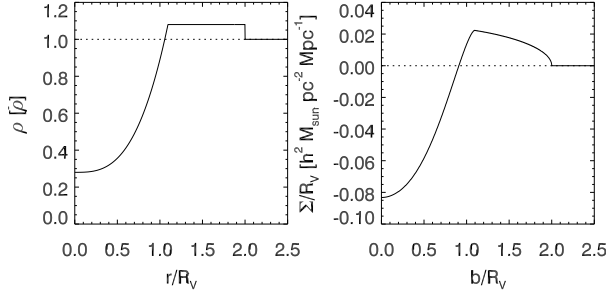


Figure 1. Left: void density profile. Right: projected void surface density scaled by R_v as the SuMIRE survey⁵, with $A = 1500$ square degrees, $n_{\text{gal}} = 20 \text{ arcmin}^{-2}$, $z_s \sim 1$, and a Euclid/WFIRST like survey with $A = 15000$ square degrees, $n_{\text{gal}} = 30 \text{ arcmin}^{-2}$, $z_s \sim 1.2$.

Throughout the paper we use the cosmological parameters derived from the *Wilkinson Microwave Anisotropy Probe* (WMAP) 7-year results (Komatsu et al. 2011).

2.1. Void Models

While voids are intrinsically ellipsoidal, we assume the averaged void density profile after stacking to be spherically symmetric. In our basic model, the void density profile and abundance follow the simulation results of Lavaux & Wandelt (2011). Specifically, we use their fitting formula

$$\rho(r, R_v) = \bar{\rho} \left(A_0 + A_3 \left(\frac{r}{R_v} \right)^3 \right) \approx \bar{\rho} \left(0.27 + 0.61 \left(\frac{r}{R_v} \right)^3 \right), \quad (1)$$

to describe the void density profile within $r = R_v$, the void radius; here $\bar{\rho}$ is the mean cosmic matter density, and where we have ignored the scatter in the best fit parameters, $A_0 = 0.27 \pm 0.01$ and $A_3 = 0.61 \pm 0.03$, which has negligible impact on our signal-to-noise calculation, assuming that the scatter is close to symmetric.

Since there are few constraints on the outer density profile of voids, we choose a continuation outside R_v with a constant density wall such that profile is compensated within $2R_v$, see Fig. 1, in order to model the extended, marginally overdense wall structures found to surround voids in recent simulations (e.g., Colberg et al. 2008; Lavaux & Wandelt 2011) and void catalogs (Sutter et al. 2012). We explore in Section 4 a range of other models, including voids surrounded by steep, overdense ridges, as found in earlier simulations and void catalogs (e.g., Pan et al. 2012). The comoving number density of voids in a $1 \text{ Mpc} h^{-1}$ wide size bin is given by (Lavaux & Wandelt 2011)

$$\frac{n_{\text{void}}(R_v \in [r, r + 1 \text{ Mpc}/h])}{(\text{Mpc}/h)^3} = 3.5 \times 10^{-3} \exp \left(-0.632 \frac{r}{\text{Mpc}/h} \right). \quad (2)$$

2.2. Weak Lensing Signals

For a lens at redshift z_l the projected surface mass density Σ is given by

$$\Sigma(\theta, R_v) = \int dr_z \left(\rho \left(\sqrt{(\theta D_A(z_l))^2 + r_z^2}, R_v \right) - \bar{\rho} \right), \quad (3)$$

where $D_A(z)$ is the proper angular diameter distance. In the linear regime, which is an excellent approximation for

the very weak lensing caused by underdense regions, the mean tangential shear γ_t and magnification μ profile of an azimuthally symmetric mass distribution are given by

$$\langle \gamma_t \rangle(\theta) = \frac{\Delta \Sigma(\theta)}{\Sigma_{\text{crit}}}, \quad \mu(\theta) \approx 1 + 2\kappa(\theta) = 1 + 2 \frac{\Sigma(\theta)}{\Sigma_{\text{crit}}}, \quad (4)$$

where κ is the lensing convergence and $\Delta \Sigma$ is the excess surface mass density defined as

$$\Delta \Sigma(\theta) = \bar{\Sigma}(\theta) - \Sigma(\theta) = \Sigma_{\text{crit}} \langle \gamma_t \rangle(\theta). \quad (5)$$

Here Σ_{crit} is the critical surface mass density weighted by the source galaxy distribution dn_s/dz_s ,

$$\Sigma_{\text{crit}} = \frac{c^2}{4\pi G} \int_{z_{s,\text{min}}}^{\infty} dz_s \frac{dn_s(z_s)}{dz_s} \frac{D_A(z_s)}{D_A(z_l)D_A(z_l, z_s)} \left(\int_{z_{s,\text{min}}}^{\infty} dz_s \frac{dn_s(z_s)}{dz_s} \right)^{-1}, \quad (6)$$

where we have neglected the narrow redshift distribution of the lens population and use the mean redshift, $z_l = 0.5$, in practice. While Bolejko et al. (2012) recently pointed out that the relativistic Doppler term arising from correlated peculiar velocities can have a significant effect on the magnification signal of source galaxies closely associated with the lensing void, this effect is negligible for our calculation due to the large separation between sources and voids, and the large number of voids used in the stacking process.

Observationally, the tangential shear is estimated as the mean tangential ellipticity of source galaxies with respect to the void center (e.g., Bartelmann & Schneider 2001). A number of techniques have been proposed to measure the magnification profile of galaxy groups and clusters; they broadly fall into two categories: magnification bias measurements, which utilize the magnification-induced variations in the apparent number density of background galaxy populations (e.g., Hildebrandt et al. 2011; Umetsu et al. 2011; Ford et al. 2012; Umetsu et al. 2012), and magnification estimators based on the change in the apparent sizes and fluxes of individual galaxies (e.g., Huff & Graves 2011; Schmidt et al. 2012). Each of these estimators is affected by a variety of systematic effects, as described in the references above; a detailed modelling of these effects is beyond the scope of this paper, and we will absorb this net irreducible observational noise into a simple one-parameter model, as described below.

In order to increase the signal-to-noise ratio (S/N) of the lensing observables, the lensing signals are measured by stacking large numbers of voids with similar sizes. In practice, the size measurement of an individual void in galaxy redshift surveys will be very noisy due to sparse sampling in the underdense region. Hence, we follow the stacking procedure of Lavaux & Wandelt (2011) and Sutter et al. (2012), who stack all voids within a size bin on their barycenters without rescaling individual voids. Ultimately, the uncertainties in the weak-lensing profiles are a combination of observational errors and cosmic noise due to projection effects of uncorrelated large-scale structure along the line of sight. The shear (magnification) profile of voids can also be written as the small-scale cross correlation function between void centers and shear (magnification), and we model their covariance matrices in analogy to galaxy-galaxy lensing (e.g. Jeong et al. 2009).

The Gaussian covariance of the angular void-shear cross

⁵ <http://sumire.ipmu.jp/>

spectrum, $C^{\gamma_i}(l) = C^{\gamma_k}(l)$ is given by

$$\text{Cov}(C^{\gamma_k}(l), C^{\gamma_k}(l')) = \frac{4\pi\delta_{ll'}^K}{A(2l+1)} \left[(C^{\gamma_k}(l))^2 + C^{\gamma\gamma} \left(C^{\kappa\kappa}(l) + \frac{\sigma_\epsilon^2}{n_{\text{gal}}} \right) + \frac{1}{n_V} \left(C^{\kappa\kappa}(l) + \frac{\sigma_\epsilon^2}{n_{\text{gal}}} \right) \right], \quad (7)$$

with $C^{\kappa\kappa}(l)$ the angular cosmic shear power spectrum, σ_ϵ^2 the ellipticity dispersion, n_V the projected number density of voids, and $C^{\gamma\gamma}(l)$ the angular void power spectrum. Note that the last term in Eq. 7 is the standard covariance estimate for stacked profiles (Hoekstra 2003). In comparison, the correlation function covariance has additional contributions from the void profile ($C^{\gamma_k}(l)$) and from void correlations ($C^{\gamma\gamma}(l)$), which increase the statistical uncertainty. The latter includes the effective increase in shape noise caused by the overlap of projected voids. For the purpose of this S/N estimate we assume voids to be unclustered; then C^{γ_k} is given by the Fourier transform of the void convergence profile, and $C^{\gamma\gamma}$ is determined by its “one-halo” term (see Cooray & Sheth 2002, for a review of the halo model). While the void density profiles used in the lensing calculations are compensated within $2R_V$, we will model projected voids as uniform disks with radius $2\theta_V$ in the calculation of the void clustering power spectrum to maximize the potential degradation caused by the projected overlap of different voids, and to avoid complications with the normalization of the halo model. Then the one-halo term of voids with angular radius θ_V and angular number density n_{θ_V} is given by

$$C^{\gamma\gamma} = \frac{1}{n_{\theta_V}} \left(\frac{J_1(2l\theta_V)}{l\theta_V} \right)^2, \quad (8)$$

with J_n the n -th order Bessel function of the first kind. For an ensemble of voids with angular radii in the range $\theta_V \in [\theta_{V,\text{min}}, \theta_{V,\text{max}}]$ and radius distribution $dn_V(\theta_V)/d\theta_V$ it is given by

$$C^{\gamma\gamma} = \left(\frac{1}{4\pi \int_{\theta_{V,\text{min}}}^{\theta_{V,\text{max}}} d\theta_V \frac{dn_V(\theta_V)}{d\theta_V} \theta_V^2} \right)^2 \times \int_{\theta_{V,\text{min}}}^{\theta_{V,\text{max}}} d\theta_V \frac{dn_V(\theta_V)}{d\theta_V} (4\pi\theta_V^2) \left(\frac{J_1(2l\theta_V)}{l\theta_V} \right)^2. \quad (9)$$

Finally, we approximate the covariance of the angular shear profile in bins $[\theta_i - \Delta\theta/2, \theta_i + \Delta\theta/2]$ with uniform bin-width $\Delta\theta$ as

$$\text{Cov}(\gamma_i(\theta_1, \Delta\theta), \gamma_i(\theta_2, \Delta\theta)) = \frac{1}{2\pi A} \int dl l J_2(l\bar{\theta}_1) J_2(l\bar{\theta}_2) \times \left[(C^{\gamma_k}(l))^2 + \left(C^{\gamma\gamma}(l) + \frac{1}{n_V} \right) C^{\kappa\kappa}(l) + C^{\gamma\gamma}(l) \frac{\sigma_\epsilon^2}{n_{\text{gal}}} \right] + \frac{\delta_{\theta_1, \theta_2}^K \sigma_\epsilon^2}{2\pi A \theta_1 \Delta\theta n_V n_{\text{gal}}}, \quad (10)$$

where the Fourier transform is evaluated at the area weighted bin centers $\bar{\theta}_i$.

Analogously, the covariance of the angular magnification

profile is given by

$$\text{Cov}(\mu(\theta_1, \Delta\theta), \mu(\theta_2, \Delta\theta)) = \frac{1}{2\pi A} \int dl l J_0(l\bar{\theta}_1) J_0(l\bar{\theta}_2) \times \left[(2C^{\gamma_k}(l))^2 + \left(C^{\gamma\gamma}(l) + \frac{1}{n_V} \right) 4C^{\kappa\kappa}(l) + C^{\gamma\gamma}(l) \frac{\sigma_\mu^2}{n_{\text{gal}}} \right] + \frac{\delta_{\theta_1, \theta_2}^K \sigma_\mu^2}{2\pi A \theta_1 \Delta\theta n_V n_{\text{gal}}}. \quad (11)$$

In the following discussion, we will refer to the two terms in Eqs. (10,11) proportional to $C^{\kappa\kappa}$ as large-scale structure noise, and to those proportional to $\sigma_{\epsilon/\mu}$ as observational noise. The contribution from the void lensing profile (C^{γ_k}) to the covariance is negligible.

Due to the high redshift of source galaxies, we assume $\sigma_\epsilon = 0.3$ per shear component. The observational noise parameter σ_μ for the magnification measurement depends on the estimator under consideration: for magnification-bias based estimators, $\sigma_\mu = 2/(q f_s^{1/2})$, where f_s is the fraction of source galaxies used in the magnification measurement, and $q \sim 1-1.5$ is a parameter describing the strength of the magnification effect related to the slopes of the galaxy luminosity and size distribution functions (Schmidt et al. 2009). For a scaling relation based estimator (Huff & Graves 2011), $\sigma_\mu = 2\sigma_\kappa/f_s^{1/2}$, with σ_κ the scatter in the convergence estimator caused by the scatter in the fundamental plane. f_s is the fraction of source galaxies to which the magnification estimator can be applied, and the factor of two propagates from convergence to magnification error. For definiteness, we use $\sigma_\mu = 2$, but note that the observational noise in the magnification estimate dominates over the large-scale structure noise, so that the error bars are proportional to σ_μ .

3. RESULTS

Fig. 2 shows the results of our calculations for the stacked void lensing profiles in different size bins, where we have assumed that the distribution of void sizes within each bin follows the form of Eq. (2). This calculation indicates that shear and magnification will provide strong constraints on the radial matter density profile of small to medium sized voids, if these can be identified from a galaxy redshift survey.

We also include the degradation of the lensing signal by stacking voids on incorrectly chosen centers, which is illustrated by the dashed lines in Fig. 2. Specifically, we assume a two-dimensional Gaussian distribution of off-center positions with variance $1 \text{ Mpc } h^{-1}$, independent of void size. Note that this illustrates the effect of severe mis-centering, as it corresponds to a rms offset of 24% of the mean void size for the smallest void size bin ($[5, 10] \text{ Mpc}/h$). Due to the shallow, slowly varying density of voids, off-centering has a much smaller impact on void lensing profiles than on cluster lensing profiles.

In Table 1 we list the radially integrated S/N for our fiducial survey, as well as for the SuMIRe and Euclid surveys. Here we have included the cosmic covariance between different radial bins, but ignored the covariance between shear and magnification measurements caused by large-scale structure as the magnification measurements are strongly dominated by observational noise.

The middle and right panels show the signal and noise expected for voids in the radius range $[5, 10] \text{ Mpc}/h$ and $[10, 15] \text{ Mpc}/h$. As can be seen from Table 1, the integrated

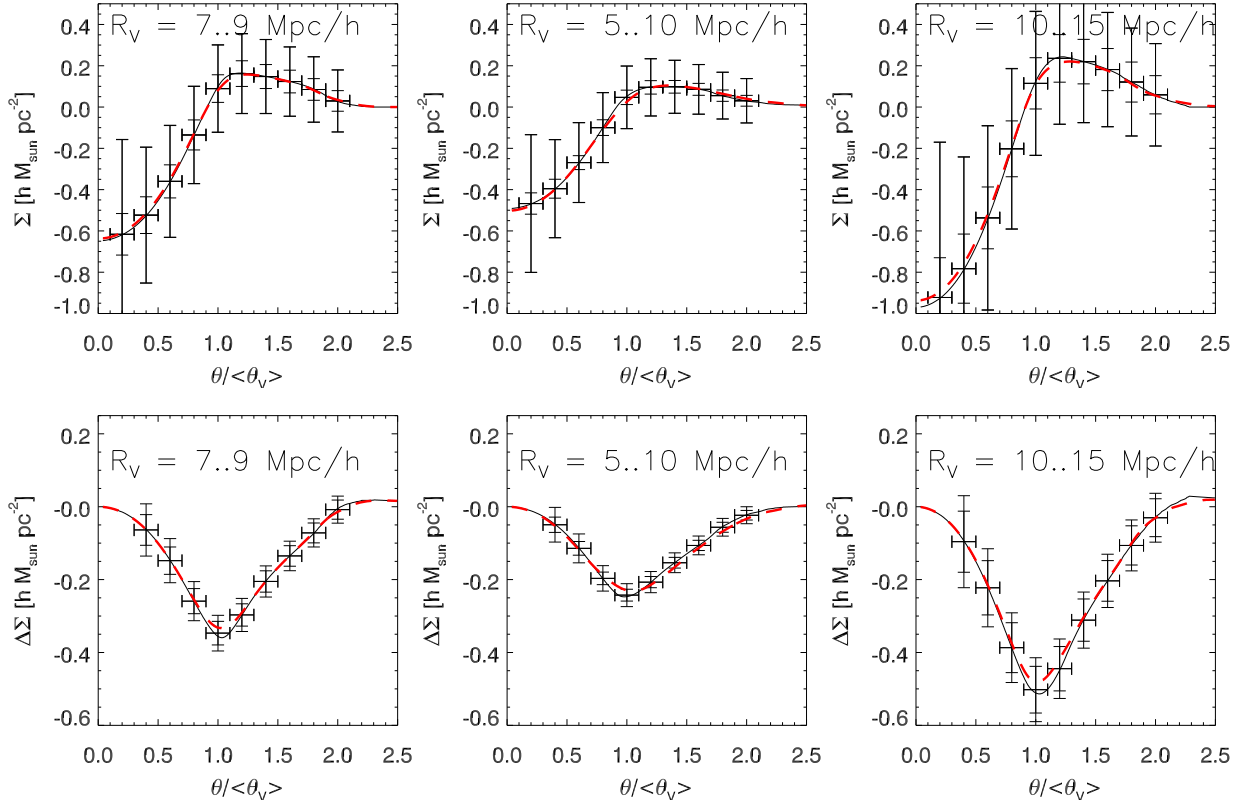


Figure 2. Void lensing profiles obtained from stacking voids in different size bins. The top panel shows the projected surface mass density Σ , which is proportional to the magnification signal. The lower panel shows $\Delta\Sigma$ (Eq. (5)), which is proportional to the mean tangential shear. The inner error bars indicate the cosmic noise contribution due to intervening large scale structure, expected for stacking voids in the redshift range $[0.4, 0.6]$ in size bins as indicated in each plot, and the larger error bars also include shape/magnification measurement noise with survey parameters described in Sect. 2. The dashed lines indicate the degradation of the lensing signal caused by stacking voids with incorrectly chosen centers, assuming a two-dimensional Gaussian distribution of off-center positions with variance $1\text{Mpc}/h$.

S/N decreases for larger voids. In our void model the amplitude of the lensing signal is linearly proportional to void size, while the noise increases more rapidly due to the exponentially decreasing void abundance. Using logarithmic size bins for the stacking cannot revert this trend. Hence, for a broad range of steeply decreasing void abundance functions, the maximum signal-to-noise will be obtained from the smallest identifiable voids.

In particular, for void sizes close to the mean spacing between galaxies, void finding algorithms may produce incomplete void catalogs. Let c denote the completeness fraction of a void catalog, such that $c = 1$ if all existing voids are identified. Then the total S/N scales as

$$S/N = (S/N)_{\text{fid}} \sqrt{c} \sqrt{\frac{A}{5000 \text{ sq dg}}}, \quad (12)$$

with our fiducial $(S/N)_{\text{fid}}$ from Table 1, which are calculated assuming $c = 1$, and A the survey area. Additionally, the S/N for magnification measurements is approximately proportional to σ_μ ,

$$(S/N)_\mu \approx (S/N)_{\mu, \text{fid}} \left(\frac{2}{\sigma_\mu} \right) \quad (13)$$

which holds as long as the error budget is dominated by observational noise ($\sigma_\mu > 0.5$). Note that these scaling require the redshift distribution of voids and background galaxies to stay constant.

Table 1
Void number density and integrated S/N for different void size bins $[R_{V, \text{min}}, R_{V, \text{max}}]$.

	$[7, 9] \text{ Mpc}/h$	$[5, 10] \text{ Mpc}/h$	$[10, 15] \text{ Mpc}/h$
$n_V, [\#/ \text{sq dg}]$	15	72	3
$(S/N)_{\text{fid}}, \gamma_t$	12	18	10
$(S/N)_{\text{fid}}, \mu$	2	3	2
$(S/N)_{\text{fid}}, \gamma_t + \mu$	12	19	11
$(S/N)_{\text{SuMIRe}}, \gamma_t$	7	10	5
$(S/N)_{\text{SuMIRe}}, \mu$	2	3	2
$(S/N)_{\text{SuMIRe}}, \gamma_t + \mu$	7	11	6
$(S/N)_{\text{Euclid}}, \gamma_t$	23	33	13
$(S/N)_{\text{Euclid}}, \mu$	8	11	7
$(S/N)_{\text{Euclid}}, \gamma_t + \mu$	24	35	15

4. DISCUSSION

The largest theoretical uncertainty of our void model is the distribution of matter around voids, that is, the transition from underdense void to filament regions. In lack of theoretical models for void density profiles we explore how well the lensing results can differentiate between a range of toy models. Specifically, we consider the following alternative models:

- Fitting function of Colberg et al. (2005), continued outside R_V with an extended, low-overdensity ridge.
- Fitting function of Lavaux & Wandelt (2011), continued outside R_V , truncated such that the void profile is compensated.

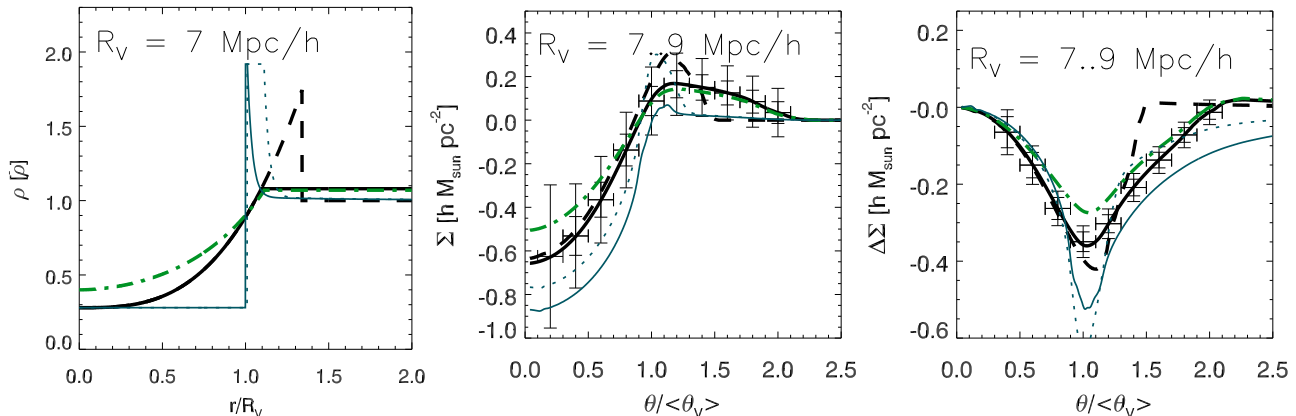


Figure 3. Impact of void density profile on lensing signal. The left panel shows our fiducial void profile, which is a compensated continuation of the fit function of Lavaux & Wandelt (2011) with an extended, low-overdensity ridge, as a thick solid line; the dashed line illustrates a compensated continuation of the same central profile with a sharp, high-density ridge; the dash-dotted line shows compensated continuation of the fit function of Colberg et al. (2005) with an extended, low-overdensity ridge, and the thin line shows an uncompensated void profile obtained from spherical expansion of an initial top-hat void profile in a Λ CDM universe. The profile illustrated by a dotted line was obtained by extending the ridge of the latter profile by hand. The middle and right panel show the stacked magnification and tangential shear signal of voids with different density profiles; error bars are the same as described in Fig. 2.

(c) Spherical top-hat density profile, evolved numerically in the Λ CDM cosmology (c.f. Sheth & van de Weygaert 2004).

(d) (c) with an artificially extended ridge.

Profile (a) is similar to our fiducial model but is less steep, having a higher central density. Profiles (b) to (d) have sharp, high-density ridges as illustrated in the left panel of Fig. 3. The resulting stacked lensing profiles are shown in the middle and right panels of Fig. 3. These results illustrate that magnification and shear signals can measure the extent of wall-structures and detect pronounced overdense ridges if these exist. However, if individual voids have sharp overdense ridges, these ridges will be smoothed out in the stacking process due to the ellipsoidal shape of individual voids. Hence to better constrain the transition between void and filament regions, in practice voids should be stacked along their projected major axis instead.

Additionally, the outer shear profile at $r \gtrsim R_v$ indicates whether the void profile is compensated or underdense: in the latter case the profile falls off like a negative point mass outside the angular extent of the void.

Also note that profiles (b) to (d) have the same central void density as our fiducial model. As the void lensing signal is affected by the outer void density profile at all projected radii, measuring the emptiness of voids from lensing observations will require parametric models of the extended void profile.

5. CONCLUSION

We have demonstrated that a DETF Stage IV type of galaxy redshift survey will allow a clear and robust detection of the stacked lensing signal of medium-sized voids with sufficient precision, $S/N \gtrsim 10$, and with $S/N \gtrsim 5$ (15) for the upcoming SuMIRE (Euclid) survey, when shear and magnification are combined, and hence provide strong direct constraints on the radial shape of the projected density profile of voids. The lensing measurement directly probes the mass distribution in and around voids, and provide an unbiased view of these underdense regions that occupy most of the cosmic volume. It will also offer new opportunities to test gravity on cosmic scales, but in under-dense regions, thus complementing cluster based tests (e.g. Lombriser et al. 2012).

We thank Peter Schneider for critical comments, and acknowledge useful discussions with Eric Huff, Bhuvnesh Jain, Peter Melchior and Fabian Schmidt. This work is supported in part by the National Science Foundation under Grant No. 1066293 and the hospitality of the Aspen Center for Physics. This research is supported in part by the National Science Council of Taiwan grant NSC100-2112-M-001-008-MY3. KU acknowledges support from the Academia Sinica Career Development Award. Part of the research described in this paper was carried out at the Jet Propulsion Laboratory, California Institute of Technology, under a contract with the National Aeronautics and Space Administration.

REFERENCES

- Albrecht, A., Bernstein, G., Cahn, R., et al. 2006, ArXiv Astrophysics e-print astro-ph/0609591
- Amendola, L., Frieman, J. A., & Waga, I. 1999, MNRAS, 309, 465
- Bartelmann, M., & Schneider, P. 2001, Phys. Rep., 340, 291
- Bolejko, K., Clarkson, C., Maartens, R., Bacon, D., Meures, N. & Beynon, E. 2012a, ArXiv e-print 1209.3142
- Bos, E. G. P., van de Weygaert, R., Dolag, K., & Pettorino, V. 2012, ArXiv e-print 1205.4238
- Colberg, J. M., Sheth, R. K., Diaferio, A., Gao, L., & Yoshida, N. 2005, MNRAS, 360, 216
- Colberg, J. M., Pearce, F., Foster, C., et al. 2008, MNRAS, 387, 933
- Cooray, A., & Sheth, R. 2002, Phys. Rep., 372, 1
- Ellis, R., Takada, M., et al, the PFS Team, 2012, ArXiv e-print 1206.0737
- Farrar, G. R., & Peebles, P. J. E. 2004, ApJ, 604, 1
- Ford, J., Hildebrandt, H., Van Waerbeke, L., et al. 2012, ApJ, 754, 143
- Hildebrandt, H., Muzzin, A., Erben, T., et al. 2011, ApJL, 733, L30
- Hoekstra, H. 2003, MNRAS, 339, 1155
- Huff, E. M., & Graves, G. J. 2011, ArXiv e-print 1111.1070
- Jeong, D., Komatsu, E., & Jain, B. 2009, Phys. Rev. D, 80, 123527
- Kamionkowski, M., Verde, L., & Jimenez, R. 2009, JCAP, 1, 10
- Komatsu, E., Smith, K. M., Dunkley, J., et al. 2011, ApJS, 192, 18
- Lavaux, G., & Wandelt, B. D. 2010, MNRAS, 403, 1392
- . 2011, ArXiv e-print 1110.0345
- Lombriser, L., Schmidt, F., Baldauf, T., et al. 2012, Phys. Rev. D, 85, 102001
- Li, B., Zhao, G.-B., & Koyama, K. 2012, MNRAS, 421, 3481
- Nusser, A., Gubser, S. S., & Peebles, P. J. 2005, Phys. Rev. D, 71, 083505
- Pan, D. C., Vogeley, M. S., Hoyle, F., Choi, Y.-Y., & Park, C. 2012, MNRAS, 421, 926
- Park, D., & Lee, J. 2007, Physical Review Letters, 98, 081301
- Peebles, P. J. E., & Nusser, A. 2010, Nature, 465, 565
- Schmidt, F., Leauthaud, A., Massey, R., et al. 2012, ApJL, 744, L22
- Schmidt, F., Rozo, E., Dodelson, S., Hui, L., & Sheldon, E. 2009, ApJ, 702, 593

Sheth, R. K., & van de Weygaert, R. 2004, MNRAS, 350, 517
Sutter, P. M., Lavaux, G., Wandelt, B. D., & Weinberg, D. H. 2012a, ArXiv
e-print 1207.2524
Umetsu, K., Broadhurst, T., Zitrin, A., Medezinski, E., & Hsu, L.-Y. 2011,
ApJ, 729, 127

Umetsu, K., Medezinski, E., Nonino, M., et al. 2012, ApJ, 755, 56